Industrial and Engineering Chemistry Research, Volume 55, Issue 35, 2016, pp. 9476-9484
DOI:10.1021/acs.iecr.6b02393

Attrition study on cement-supported biomass-activated calcium sorbents for CO_2 capture

Lunbo Duan *[,†,‡], Zhijian Yu [†], María Erans [‡], Yingjie Li [§], Vasilije Manovic [‡], Edward J. Anthony [‡]

[†] Key Laboratory of Energy Thermal Conversion and Control, Ministry of Education, School of Energy and Environment, Southeast University, Nanjing 210096, China

[‡] Combustion and CCS Centre, Cranfield University, Bedfordshire, MK43 0AL, UK

[§] School of Energy and Power Engineering, Shandong University, Jinan 250061, China

Abstract

Enhanced CO_2 capacity of biomass modified Ca-based sorbent has been reported recently, but undesired attrition resistance has also been observed. Cement was used as a support for biomass-activated calcium sorbent during the granulation process in this study, in order to improve the poor mechanical resistance. Attrition tests were carried out in an apparatus focused on impact breakage to evaluate how the biomass addition and cement support influence the particle strength during Ca-looping. Results showed biomass addition impaired the mechanical strength and cement support could improve it, which is reflected by the breakage probability and size change after impact of pellets experienced calcination and multiple calcination/carbonation cycles. Larger-sized particles suffered more intense attrition. The mechanical strength of sorbents declined significantly after higher temperature calcination but increased after carbonation. After multiple cycles, the mechanical strength of particles was greatly enhanced, but more cracks emerged. A semi-empirical formula for calculating average diameter after attrition based on Rittinger's surface theory was developed. Observation on the morphology of particles indicated that particles with more porosity and cracks were more prone to breakage.

Key words: Calcium sorbent; biomass-activated; cement-supported; calcination/carbonation cycle; attrition

1. Introduction

The calcination/carbonation cycles of calcium-based sorbents (also called calcium looping, or CaL) in dual fluidised bed systems represents a viable method to capture CO_2 from fossil fuel-fired power

plants[1-3]. However, during operation, two main problems occur: continuous reactivity decay[4-6] due to the loss of micro- and meso-pores; and serious elutriation[7-10] resulting from size reduction of the sorbent particles because of attrition. The latter occurs when the particles suffer wear during collision with other particles and the reactor walls. Elutriation reduces the residence time of the particles in the furnace, increasing sorbent make-up rates and the consequent overall costs. Solving these problems requires improvements in reactivity and mechanical stability. However, often very reactive particles are not strong enough to survive in the high temperature and turbulent flow, while strong particles may not be reactive enough to capture CO_2 in a short time.

Many methods have been proposed to improve sorbent reactivity, as summarised by Valverde[11]: the use of rigid porous materials as carriers of the Ca-based sorbents, use of additives to improve the sorbent thermal stability, reduction of the sorbent particle size down to the nanometre scale, and use of synthetic precursors to produce novel sorbents with a rich micro-pore structure. Recently, Chen et al.[12] reported calcium-based sorbent doped with metal oxides through the sol-gel process possessed enhanced reactivity by distributing metal oxides into molecular scale. Pressurized carbonation was beneficial for CO_2 capture also could be found in Chen's work[13]. Among these, biomass additives[14] serve as a cheap and efficient way to elevate the reactivity of the calcium sorbent, by improving the pore structure through biomass combustion. Also, the ash after combustion may serve as a composite framework. Our recent work[15] confirmed that biomass-activated calcium pellets (limestone + biomass) have better CO_2 capture performance than other tested pellets (limestone + cement, and limestone + biomass + cement) in a thermogravimetric analyser (TGA). Interestingly, results obtained from a bubbling fluidised bed were not the same and the biomass-activated pellet showed the poorest performance. This is presumably because of material loss due to attrition under fluidised bed (FB) conditions. It is well known that cement is a good support for calcium-based sorbents[15-19] and the reaction between CaO and alumina (Al_2O_3) to form mixed calcium–aluminium oxides (e.g., mayenite) results in the formation of an inert solid binder. The binder serves to reduce sintering of the CaO grains by providing an inert framework and to improve the mechanical stability of the sorbent[16].

There are several methods to evaluate thermal stability of sorbent materials. The most common and direct method[20-22] is to carry out the test in a fluidised bed and measure the particle size of the materials after a number of reaction cycles. This method yields a number for attrition, but detailed information and the mechanism cannot be easily obtained since there are too many contributing factors.

A Standard Test Method for Determination of Attrition and Abrasion of Powdered Catalysts by Air Jets (D5757 – 00) proposed by the American Society for Testing and Materials (ASTM) has also been used[23-25] to evaluate the attrition properties of calcium-based sorbents through an Air Jet Index (AJI, a unitless index numerically equal to the percent attrition loss at 5 hour). However, this method provides general information, obtained in a spouted bed, rather than a bubbling or fast bed, usually used in the calcium looping process. Scala *et al*.[26-29] proposed a single particle impact apparatus, in which particles accelerated by the gas stream strike a target, to test different limestone after calcination, desulphurisation and hydration. This setup was focused on attrition by impact damage which is frequent in fluidised beds. Although the device could not simulate the entire attrition history of particles, the attrition resistance could be evaluated more accurately by this approach.

In this work, a similar system to Scala's was developed to investigate the attrition behaviour of different calcium-based sorbents and evaluate how the biomass addition and cement support influence the mechanical strength of the sorbent. The effects of particle size, calcination temperature, carbonation and multiple calcination/carbonation cycles on attrition resistance of sorbents were performed. The relationship between morphology characteristics and strength of sorbents was also fully explored.

2. Experimental

2.1. Sample preparation

Longcal SP52 limestone from the UK, less than 125 μm was calcined at 850°C in a muffle furnace for two hours. The product was then mixed with commercial flour (as the biomass binder used in this paper) and a portion was mixed with calcium aluminate cement (CA-14 from Almatis Inc.).

The mixture was poured into a TMG Tabletop mechanical granulator provided by Glatt GmbH to produce the sorbent pellets. The volume of the pelletiser vessel was 4 L, and the velocities for the agitator and the chopper were 500 rpm and 2500 rpm, respectively. About 1 L of deionized water was sprayed progressively during the operation. Then, the particles were air dried for 12 h before being stored in a desiccator to avoid any reactions of the material with air.

Three types of pellets were prepared and named according to their compositions: the calcined limestone modified by addition of 10 wt.% flour (LF); the calcined limestone with 10 wt.% aluminate cement added (LC); and the calcined limestone mixed with 10 wt.% flour and 10 wt.% cement (LCF).

The constituents of pellets are shown in Table 1 and the compositions measured by X-ray fluorescence (XRF) are shown in Table 2. The increase of K_2O mass in the LF and LCF samples seen in Table 2 indicates the flour contains abundant potassium, which has been reported to be beneficial for reactivity improvement[30]. The CO_2 capture performance of these sorbents was reported in reference 15.

Table 1. Constituents of sorbents (wt. %)

Component	LF	LC	LCF
Calcined limestone	90	90	80
Cement	-	10	10
Flour	10	-	10

Table 2. Composition of sorbents (wt. %) by XRF

Sample	CaO	Al_2O_3	K_2O	MgO	SiO_2	Others	LOI
Limestone	55.0	0.084	0.007	0.189	0.715	0.230	43.78
LF	56.1	0.210	0.036	0.202	0.742	0.255	42.46
LC	57.9	5.585	0.006	0.206	1.190	0.254	34.86
LCF	50.4	4.552	0.022	0.190	0.257	0.176	44.40

LOI = Loss on ignition.

2.2. Apparatus and procedures

Calcination, carbonation and CaL cycles of samples were carried out in a bubbling fluidised bed reactor, as shown in Figure 1. The reactor consists of a quartz reaction vessel heated by a two-stage external-resistance furnace. The first stage is used to preheat the gas to 300 ^oC and the second stage is to control the temperature of reaction. The quartz reaction vessel has an inner diameter of 25 mm and length of 1800 mm. The gas distributor is a sintered plate. The height from the top of the reactor to the air distributor is 1000 mm. Fluidisation gas, premixed using a mass flowmeter controller, was supplied from the bottom of the reactor. The concentration of CO_2 during carbonation was analysed by a non-dispersive infrared analyser (Rosemount, NGA 2000) whose CO_2 range and precision was 50% and 0.5%, respectively.

The impact testing of the pellets was performed in the impact apparatus shown in Figure 2. The setup, in which particles accelerated by the gas stream hit a target, takes advantage of the approach

proposed by Scala et al.[26-29]. The feeding unit is installed at the top and consists of two valves. The first valve is closed after feeding to prevent the gas from escaping. The particles are stored in the hopper with a 1 mm i.d. at the bottom section, so they stack vertically. The second valve (gate valve) controls the particles such that they fall into the eductor one by one. The eductor is 1.1 m long and 10 mm i.d. The gas flows into the tube from the side and velocity is controlled by a mass flow meter. The particles, accelerated by the gas flow and gravity, impact a stainless target at the bottom of the system. The target is set into the collection chamber 30 mm below the end of the tube. The target is inclined by 60° with respect to the vertical. The inclination was chosen by considering the effect of rebounding particles. The chamber, 200 mm high and 200 mm i.d., is made of transparent Plexiglas which is suitable for use with a high-speed camera to track the particles location and by this the particle velocity can be measured. The results show that the particle was accelerated to nearly the gas velocity before it reached the target plate. The top section of the chamber is a sintered porous metal plate which can filter the entrained fine particles from the escaping gas. The chamber can be taken apart to allow collection of the particles after impact for further analysis.

The particles to be subjected to the impact test (described above) were obtained from the sorbent after calcination/carbonation tests in a FB reactor. About 25 g of pellets of size range 0.4-0.6 mm were weighed for each FB test. Bed material was not used in these experiments. The first calcination was carried out at 850 ^{o}C in N_2 or 950 ^{o}C in CO_2 for LF and LCF to decompose the biomass. Multiple CaL cycles were carried out by calcining the sample at 850 ^{o}C for 15 min in pure N_2 and carbonating it at 650 ^{o}C for 20 min in 15% v/v CO_2, balance N_2. The fluidisation number (U/U_{mf}) was about 4 and the fluidisation velocity was 0.6 m/s. The gas volume flow rate through the flowmeter was calibrated at different temperatures based on the state equation of ideal gas. The product was then sieved in the particle size range of 0.35-0.5 mm for impact tests.

About 2 g of pellets were used for each impact test at room temperature. The impact velocities were 5, 10, 18, 26, and 34 m/s, conforming to particle impact conditions near the gas distributor, in the bed and cyclone. According to the calculations, the particles approach terminal velocity after accelerating through the eductor (1.1 m length). The terminal velocity was equal to the gas velocity plus free falling velocity of the particle. For particle size of 0.4 mm or less, the free falling velocity is so small that it can be ignored in comparison to the gas velocity. If the mass of fragments collected after the impact test deviated by less than 1% from initial mass, the test was seen as satisfactory. Debris was sieved to

determine the size distribution after each impact. Three parallel tests were performed to guarantee the reproducibility of the results for parts of the experiments.

The definition of breakage probability[31], *f*, is given by Eq. (1). Using Eq. (2) and Eq. (3) the Sauter mean diameter (d_{sv}) and size reduction of d_{sv} are calculated. The probability density function (PDF) of particle size (PSD) is calculated by Eq. (4) to describe the size distribution of particles.

$$f = \frac{m_{Debris}}{m} \tag{1}$$

$$d_{sv} = \frac{1}{\sum x_i / d_{pi}} \tag{2}$$

$$I = \frac{d_0 - d_{sv}}{d_0} \times 100\% \tag{3}$$

$$PDF_i = \frac{x_i}{d_{pi}} \tag{4}$$

where m_{Debris} is the mass of debris whose size falls below the lower limit of the feed size interval; m is the total mass of particles; x_i is the mass fraction of particles in size interval of i; d_{pi} is the length of size interval of i; and d_0 is the initial mean size.

Morphology observation and microstructure tests were also done to study the potential relationship between structure and mechanical strength. The pore microstructure was measured by nitrogen adsorption/desorption isotherm tests at -196.8 ^{o}C on a Micromeritics ASAP 2020-M analyser. The morphology was observed with a scanning electron microscope (SEM).

3. Results and discussion

3.1. Impact fragmentation of the raw sorbents

The breakage probability of raw sample LF, LC, LCF and limestone of size range of 0.35-0.5 mm at different impact velocities is shown in Figure 3. The pellets subjected to higher speed suffer more intense breakage since they have larger momentum. The breakage probability of LF is 4.2%-17.1% at impact velocity range of 5-34 m/s, respectively, while the breakage probability of LC is 0.3%-6.7% over the same velocity range. Although the addition of biomass is beneficial for enhancing reactivity, it weakens the pellet strength. The breakage probability of LCF is 1.5%-11.2% at impact velocity range of 5-34 m/s, indicating the addition of cement can improve the rigidity of sorbents significantly at room temperature compared to LF pellets since the cement serves as only a physical binder and skeleton at this temperature. The LCF pellet, which is prepared by mixing biomass in a commercial pelletisation method can be an available candidate for CO_2 capture since it possesses both reliable

reactivity[15] and mechanical strength. The raw limestone and LC retain similar breakage probability at room temperature, except for a small deviation at 26-34 m/s. It seems that cement-supported sorbent can reach the strength of the original limestone.

The breakage probability of LC in the size ranges of 0.35-0.5 mm, 0.5-0.6 mm and 0.6-0.85 mm at different impact velocities is exhibited in Figure 4. The fragmentation of pellets of the same material is sensitive to particle size, and particles with larger size suffer more intense breakage.

Using the Griffith Equation, Eq. (5)[32], the critical stress of breakage can be acquired.

$$\sigma_f = \sqrt{2E\gamma_S / \pi c} \tag{5}$$

where, σ_f is critical breaking stress; E is Young's modulus; γ_S is surface energy of material; and $2c$ is the length of crack (equal to particle size when particle splits entirely). The σ_f increases as the particle size decreases since the E and γ_S are constant for the same material. For fragmentation to occur, larger particles usually require big cracks as well as smaller critical stress. Meanwhile, there exists a minimum size below which the critical stress cannot be reached and the particles are difficult to break further.

3.2. Effect of calcination

Figure 5a displays the breakage probability of LF, LC, LCF and limestone calcined at 850 ^{o}C and 950 ^{o}C for 15 min (simulating the first calcination during calcium looping) at different impact velocities. The reduction of Sauter mean diameter versus impact velocity is shown in Figure 5b. All calcined samples show higher breakage probability than raw pellets for all tested impact velocities. This means that the mechanical strength of sorbents declines after calcination[26-27]. Furthermore, the curves of all samples calcined at 950 ^{o}C are above those calcined at 850 ^{o}C, which indicates that Ca-based sorbents suffer more from fragmentation at higher temperature. The internal pressure stress, caused by the hindering of gas flow through the particle, and thermal stress are usually more notable at higher calcination temperature, which generates cracks at the surface of samples and plays a vital role in diminution of particle strength.

The breakage probability at impact velocity range of 5-34 m/s decreases from 6.8%-46.1% for LF to 3.5%-22.9% for LCF and the reduction of Sauter mean size decreases from 5.0%-38.9% for LF to 4.1%-22.4% for LCF. Calcined LF is more prone to fragment, while LCF containing cement shows

much better attrition resistance.

Manovic and Anthony[16], along with other workers[33, 35] have noted that some of the CaO from limestone could react with the cement to form calcium aluminates at calcination temperature, like $Ca_{12}Al_{14}O_{33}$ (mayenite) or $Ca_3Al_2O_6$, for different Ca/Al ratios. The surface morphology of LCF after first calcination at 850 °C is shown in Figure 6. The appearance of calcium aluminate in Figure 6 is similar to the images found elsewhere in the literature[33, 34]. Calcium aluminate forms a stable cross-linked nano-sized framework and CaO grains are embedded in the framework. So, unconsolidated grains are connected by those chemical bonds and a tougher structure is acquired. The porous channels generated by the decomposition of biomass and $Ca(OH)_2$ can also be observed. This property leads to the poorer attrition resistance of LCF than LC.

Compared to limestone, LC suffers marginally higher breakage probability and reduction of Sauter mean size after calcination at different temperatures. This result agrees well with the worse attrition resistance of calcined cement-supported pellets than that of lime tested by an Air Jet apparatus from Knight et al.[23]

Figure 7 reports the probability density function of the sizes (PSD) of LF and LCF collected after impact. For both samples, the mass of particles in the feeding size range decreases noticeably, while mass of particles increases in size interval of 0-0.2 mm and 0.3-0.35 mm. Scala et al.[26] identified three kinds of typical breakage pattern which can be identified by the size distribution of fragments. Based on this concept, the calcined pellets of LF and LCF mostly undergo splitting (breakage into a relatively small number of fragments of a size comparable with the parent particle size), combined with moderate disintegration (extensive loss of particle connectivity, which results in the generation of a large number of small fragments) while the LCF pellets suffer less disintegration since the strength has been improved.

3.3. Effect of multiple calcination/carbonation cycles

3.3.1. Effect of multiple calcination

LCF and LC are used to carry out 5 and 11 calcination/carbonation cycles. LF was not included due to its poorer strength. To facilitate the following attrition test, the final step of the last cycle is calcination. The size range of the samples on which the impact tests were performed is 0.35-0.5 mm. Figure 8a reports the breakage probability of samples experiencing a different number of cycles. The

breakage probability of LC and LCF at impact velocity range of 5-34 m/s are 1.5%-10.9% and 3.5%-22.9% after the first calcination, 0.9%-9.2% and 3.0%-18.7% after the 5th calcination and 0.7%-6.1% and 2.1%-14.0% after the 11th calcination, respectively. Figure 8b reports the corresponding reduction of Sauter mean diameter of LCF and LC. They decrease from 4.1%-22.4% and 0.6%-8.6% after the first calcination to 0.8%-10.4% and 0.2%-4.9% after the 11th calcination, respectively. It can be concluded that the attrition resistance is enhanced gradually after multiple calcinations.

Carbonation causes swelling of CaO as a result of the change of the molar volume from 16.9 $cm^3 \cdot mol^{-1}$ for CaO to 37.0 $cm^3 \cdot mol^{-1}$ for $CaCO_3$. Chemical stress is obvious at the surface of particles during swelling. The calcination of $CaCO_3$ results in excess internal pressure stress, which is greater than the critical stress of sorbents. So cracks inside and at the surface of particles emerge as the effect of iterative stress. The significantly increased cracks were observed in SEM images presented in the following section. According to Griffith's work[35], stress concentration will occur near cracks in solid materials. Therefore, particles with more cracks will suffer more attrition. Also the porosity caused by the decomposition of biomass and $Ca(OH)_2$ contributes to the breakage of the pellets.

Figure 9 illustrates the surface morphology of LCF after the 11th calcination. Compared with Figure 6, the grains merge together and the number of porous channels decreases. It should be noted that this property could be caused by the combined effect of sintering and further CaO/Al_2O_3 reaction. A more compact structure forms and it is more difficult to split this structure into smaller particles. The strength improvement by grains merging and the decline of cracks, means that the effect of grains merging is more important after multiple cycles because the total attrition resistance is enhanced.

3.3.2. Effect of multiple carbonation

Figure 10a indicates the breakage probability of samples after the first and 11th carbonation; the corresponding reduction of Sauter mean diameter can be seen in Figure 10b. Comparing to the results in Figure 5a, the breakage probability range of 5-34 m/s is 1.0%-9.2%, 4.3%-29.7% and 3.1%-19.1% for LC, LF and LCF after the 1st carbonation, respectively, which are lower than the calcined results of 1.5%-10.9%, 6.8%-46.1% and 3.5%-22.9%. Recarbonation is effective in reducing the impact damage propensity of the sorbent because the $CaCO_3$ shell can resist impact and the hardness of $CaCO_3$ is greater than CaO[24].

The mechanical resistance of samples is enhanced after multiple carbonations. The reason is also the

competitive effect between grains merging and increased cracks.

Figure 11 illustrates the probability density function of size of LCF after the 11th carbonation and 11th calcination. The mass fraction of particles in the feeding size range decrease, while the particle fractions in the size ranges of 0.3-0.35 mm and 0.15-0.25 mm increase slightly. The breakage pattern of LCF after the 11th carbonation and calcination is mostly chipping (producing a few fragments of size much smaller than the mother particles) as a result of the enhanced strength caused by grains merging.

3.4. Modelling of attrition

Rittinger's surface theory[36] illustrates that the generation of new surface area of impacted particles is proportional to the total kinetic energy consumed. Chen et al.[37] reported that the impact attrition of limestone particles followed this theory and a three-parameter attrition model described as Eq. (6) was proposed:

$$\frac{d_0}{d_{sv}} = k_{Imp} v^2 N + \gamma \tag{1}$$

where, d_0 is average diameter of feeding particle; d_{sv} is Sauter mean size after impact; k_{Imp} is the pre-factor which can reflect the strength of particles; v is the impact velocity of particle; N is the number of impact cycles; and γ is a constant.

Table 3. Model coefficients of impact attrition for LCF

Samples	Confidence intervals				Correlation coefficient R^2
	$k_{Imp} \times 10^4$ (s^2/m^2)	Deviation	γ (unitless)	Deviation	
Raw LCF	0.516	±0.095	1.0074	±0.0059	0.9656
Calcination at 850 °C	2.23	±0.311	1.0430	±0.0192	0.9800
Calcination at 950 °C	2.75	±0.782	1.0871	±0.0483	0.9206
After 1st carbonation	1.63	±0.113	1.0115	±0.0070	0.9950
After 5th calcination	1.65	±0.124	1.0245	±0.0077	0.9942
After 11th calcination	0.935	±0.079	1.0098	±0.0049	0.9925

* 95% confidence

In this paper, N=1 since impact cycles are not used. Figure 12 shows the relationship between d_0/d_{sv} of LCF before and after different reactions vs. the square of the impact velocity. It can be seen that

d_0/d_{sv} varies almost linearly with v^2. Least-square-fitting was performed based on Eq. (6) and the model coefficients of impact attrition are listed in Table 3. Confidence of 95% is employed in calculating confidence interval of parameters.

The correlation coefficient (R^2) from Table 3 for all conditions has an average value of 0.9747. This means the impact attrition of both raw LCF and LCF after calcination or multiple cycles also conforms to Rittinger's surface theory. The average diameter of those particles after impact in unknown but velocities can be calculated by Eq. (6) and the accuracy can be guaranteed. Smaller k_{Imp} reflects higher strength of particles based on Chen's research[37]. Therefore, the raw pellets possess the highest strength since the k_{Imp} is 0.516×10^{-4} s^2/m^2, which declines after calcination to 2.75×10^{-4} s^2/m^2. The k_{Imp} of pellets after the 11th calcination is 0.935×10^{-4} s^2/m^2, which means the strength has increased.

3.5. Microstructure analysis

Figure13 presents the surface area and pore volume distributions of sorbents during multiple cycles. According to Figure13a, although LC possesses higher Brunauer-Emmett-Teller (BET) surface area at the initial cycle, it suffers a more severe surface area decrease after multiple cycles. Figure 13b and Figure 13c suggest the general pore volume of both samples declines after multiple reactions. The pore volume of LC reaches a much lower level after the 11th cycle than that of LCF which undergoes less decrease. Mesopores (2-50 nm) are beneficial for CO_2 capture, so less change in pore volume for LCF suggests slower decay of CO_2 capture capacity after cycles than LC which is consistent with the results reported in section 3.1.

Although pore diameter higher than 300 nm cannot be approached by N_2 absorption/desorption, it is apparent that grain merging occurs inside pellets after long durations of high-temperature reaction since CO_2 capacity declines. Also the decrease of porosity produces more compact structures which can enhance the mechanical resistance.

The SEM images of sorbent pellets are presented in Figure 14. Figure 14a indicates that LF has a rugged and unconsolidated surface after the first calcination at 850 ^oC. Figure 14b shows LF possesses ample pores of large size caused by burning out of biomass, so the connection between grains is weak. This characteristic results in a low level of strength. The effect caused by adding cement in LF is prominent, which can be found from Figure 14c. The calcined LCF has a smooth and compact surface, unlike LF, which can improve attrition resistance. Comparing Figure 14c and Figure 14d, larger and

more numerous cracks are generated on the sorbent's surface after first calcination at 950 ^{o}C. By comparing Figure 14c with Figure 14e, it is apparent that more cracks emerge and the average size increases after the 11th calcination, and the cracks are unfavorable to reduce attrition since stress concentration and breakage will occur along such cracks. Biomass addition does not influence the morphology structure significantly since the calcined LC and LCF show the same surface properties, as shown in Figure 14e and Figure 14f.

4. Conclusion

All of the modified lime-based sorbents for high-temperature CO_2 capture were granulated with a mechanical pelletiser. Impact tests were performed on both fresh material and the materials after multiple CaL cycles. Results showed that introducing biomass was detrimental to the fragmentation resistance of the pellets, but the addition of cement could enhance the otherwise unsatisfactory mechanical strength. The smaller sized particles were more resistant to fragmentation. The attrition resistance of sorbents declined significantly after higher temperature calcination but was elevated after recarbonation and multiple cycles. The conversion of the major particle failure pattern from "splitting" after calcination to "chipping" after multiple cycles was observed. The impact attrition of LCF also conforms to the theory that the area of new surface generated is approximately proportional to impact kinetic energy. Morphology analysis of particles indicated Cracks caused by chemical stress during calcination and multiple cycles will impair the mechanical resistance, while compact structure with less porosity can endure higher impact load.

Acknowledgement

Financial support from National Natural Science Foundation of China through Grant No. 51206023 and funding from the European Community's Research Fund for Coal and Steel (RFCS) under grant agreement No. RFCR-CT-2012-00008 are gratefully acknowledged.

Author information

Corresponding Author

* Tel.: +86-25-83790147. E-mail address: duanlunbo@seu.edu.cn (L. Duan).

Notes

The authors declare no competing financial interest.

References

(1) Li, F.; Fan, L. S. Clean coal conversion processes–progress and challenges, *Energy Environ. Sci.* **2008**, *1*, 248-267.

(2) Blamey, J.; Anthony, E. J.; Wang, J.; Fennell, P. S. The calcium looping cycle for large-scale CO_2 capture. *Prog. Energy Combust. Sci.* **2010**, *36*, 260-279.

(3) Zhao, C.; Chen, X.; Anthony, E. J.; Jiang, X.; Duan, L.; Wu, Y. Capturing CO_2 in flue gas from fossil fuel-fired power plants using dry regenerable alkali metal-based sorbent. *Prog. Energy Combust. Sci.* **2013**, *39*, 515-534.

(4) Lysikov, A. I.; Salanov, A. N.; Okunev, A. G. Change of CO_2 carrying capacity of CaO in isothermal recarbonation-decomposition cycles. *Ind. Eng. Chem. Res.* **2007**, *46*, 4633-4638.

(5) Alonso, M.; Rodríguez, N.; González, B.; Grasa, G.; Murillo, R.; Abanades, J. C. Carbon dioxide capture from combustion flue gases with a calcium oxide chemical loop. Experimental results and process development. *Int. J. Greenhouse Gas Contr*. **2010**, *4*, 167-73.

(6) Wang, C.; Zhou, X.; Jia, L.; Tan, Y. Sintering of Limestone in Calcination Carbonation Cycles. *Ind. Eng. Chem. Res.* **2014**, *53*, 16235-16244.

(7) Fennell, P. S.; Pacciani, R.; Dennis, J. S.; Davidson, J. F.; Hayhurst, A. N. The effects of repeated cycles of calcination and carbonation on a variety of different limestones, as measured in a hot fluidized bed of sand. *Energy Fuels* **2007**, *21*, 2072-2081.

(8) Charitos, A.; Hawthorne, C.; Bidwe, A. R.; Sivalingam, S.; Schuster, A.; Spliethoff, H.; Scheffknecht, G. Parametric investigation of the calcium looping process for CO_2 capture in a 10kW th dual fluidized bed. *Int. J. Greenhouse Gas Contr.* **2010**, *4*, 776-784.

(9) Coppola, A.; Scala, F.; Salatino, P.; Montagnaro, F. Fluidized bed calcium looping cycles for CO2 capture under oxy-firing calcination conditions Part 1. Assessment of six limestones, *Chem. Eng. J.* **2013**, *231*, 537-543.

(10) Wu, Y.; Manovic, V.; He, I.; Anthony, E. J. Modified lime-based pellet sorbents for high-temperature CO_2 capture: reactivity and attrition behavior. *Fuel* **2012**, *96*, 454-461.

(11) Valverde, J. M. Ca-based synthetic materials with enhanced CO_2 capture efficiency. *J. Mater. Chem. A* **2013**, *1*, 447-468.

(12) Chen, H.; Zhang, P.; Duan, Y.; Zhao, C. Reactivity enhancement of calcium based sorbents by doped with metal oxides through the sol–gel process. *Appl. Energy* **2016**, *162*, 390-400.

(13) Chen, H.; Zhao, C.; Yang, Y.; Zhang, P. CO_2 capture and attrition performance of CaO pellets with aluminate cement under pressurized carbonation. *Appl. Energy* **2012**, *91*, 334-340.

(14) Ridha, F. N.; Wu, Y.; Manovic, V.; Macchi, A.; Anthony, E. J. Enhanced CO_2 capture by biomass-templated $Ca(OH)_2$-based pellets. *Chem. Eng. J.* **2015**, *274*, 69-75.

(15) Erans, M.; Beisheim, T.; Manovic, V.; Jeremias, M.; Patchigolla, K.; Dieter, H.; Duan, L.; Anthony, E. J. FDCCS16 Effect of SO_2 and steam on CO_2 capture performance of biomass-templated calcium aluminate pellets. *Faraday Discuss* **2016**.

(16) Manovic, V.; Anthony, E. J. CaO-based pellets supported by calcium aluminate cements for high-temperature CO_2 capture. *Environ. Sci. Technol*. **2009**, *43*, 7117-7122.

(17) Manovic, V.; Anthony, E. J. Long-term behavior of CaO-based pellets supported by calcium aluminate cements in a long series of CO_2 capture cycles. *Ind. Eng. Chem. Res*. **2009**, *48*, 8906-8912.

(18) Ridha, F. N.; Manovic, V.; Macchi, A.; Anthony, E. J. CO_2 capture at ambient temperature in a fixed bed with CaO-based sorbents. *Appl. Energy* **2015**, *140*, 297-303.

(19) Manovic, V.; Wu, Y.; He, I.; Anthony, E. J. Spray water reactivation/pelletization of spent CaO-based sorbent from calcium looping cycles. *Environ. Sci. Technol*. **2012**, *46*, 12720-12725.

(20) Jia, L.; Hughes, R.; Lu, D.; Anthony, E. J.; Lau, I. Attrition of calcining limestones in circulating fluidized-bed systems. *Ind. Eng. Chem. Res.* **2007**, *46*, 5199-5209.

(21) Zhang, W.; Li, Y.; Duan, L.; Ma, X.; Wang, Z.; Lu, C. Attrition behavior of calcium-based waste during CO_2 capture cycles using calcium looping in a fluidized bed reactor. *Chem. Eng. Res. Des.* **2016**, *109*, 806-815.

(22) Materic, V.; Hyland, M.; Jones, M. I.; Holt, R. Investigation of the friability of Ca looping sorbents during and after hydration based reactivation. *Fuel* **2014**, *127*, 70-77.

(23) Knight, A.; Ellis, N.; Grace, J. R.; Lim, C. J. CO_2 sorbent attrition testing for fluidized bed systems. *Powder Technol*. **2014**, *266*, 412-423.

(24) Xiao, G.; Grace, J. R.; Lim, C. J. Evolution of Limestone Particle Size Distribution in an Air-Jet Attrition Apparatus. *Ind. Eng. Chem. Res.* **2014**, *53*, 15845-15851.

(25) Valverde, J. M.; Quintanilla, M. A. S. Attrition of Ca-based CO_2-adsorbents by a high velocity gas jet. *AIChE J.* **2013**, *59*, 1096-1107.

(26) Scala, F.; Montagnaro, F.; Salatino, P. Attrition of limestone by impact loading in fluidized beds. *Energy Fuels* **2007**, *21*, 2566-2572.

(27) Scala, F.; Salatino, P. Flue gas desulfurization under simulated oxyfiring fluidized bed combustion conditions: The influence of limestone attrition and fragmentation. *Chem. Eng. Sci.* **2010**, *65*, 556-561.

(28) Montagnaro, F.; Salatino, P.; Santoro, L.; Scala, F. The influence of reactivation by hydration of spent SO_2 sorbents on their impact fragmentation in fluidized bed combustors. *Chem. Eng. J.* **2010**, *162*, 1067-1074.

(29) Coppola, A.; Palladino, L.; Montagnaro, F.; Scala, F.; Salatino, P. Reactivation by Steam Hydration of Sorbents for Fluidized-Bed Calcium Looping. *Energy Fuels* **2015**, *29*, 4436-4446.

(30) González, B.; Blamey, J.; McBride-Wright, M.; Carter, N.; Dugwell, D.; Fennell, P.; Abanades, J. C. Calcium looping for CO_2 capture: Sorbent enhancement through doping. *Energy Procedia* **2011**, *4*, 402-409.

(31) Samimi, A.; Moreno, R.; Ghadiri, M. Analysis of impact damage of agglomerates: effect of impact angle. *Powder Technol.* **2004**, *143*, 97-109.

(32) Shipway, P. H.; Hutchings, I. M. Attrition of brittle spheres by fracture under compression and impact loading. *Powder Technol*. **1993**, *76*, 23-30.

(33) Wu, S. F.; Jiang, M. Z. Formation of a $Ca_{12}Al_{14}O_{33}$ nanolayer and its effect on the attrition behavior of CO_2-adsorbent microspheres composed of CaO nanoparticles. *Ind. Eng. Chem. Res*. **2010**, *49*, 12269-12275.

(34) Luo, C.; Zheng, Y.; Ding, N.; Zheng, C. Enhanced cyclic stability of CO_2 adsorption capacity of CaO-based sorbents using La_2O_3 or $Ca_{12}Al_{14}O_{33}$ as additives. *Korean J. Chem. Eng.* **2011**, *28*, 1042-1046.

(35) Anderson, T. L. *Fracture mechanics: fundamentals and applications;* CRC press: New York, 2005.

(36) Ray, Y. C.; Jiang, T. S.; Wen, C. Y. Particle attrition phenomena in a fluidized bed. *Powder Technol.* **1987**, *49*, 193-206.

(37) Chen, Z.; Lim, C. J.; Grace, J. R. Study of limestone particle impact attrition. *Chem. Eng. Sci.* **2007**, *62*, 867-877.

Figure captions

Fig 1. Scheme of the bubbling fluidised bed

Fig 2. Impact apparatus diagram

Fig 3. Breakage probability of different samples versus impact velocity (particle size range of 0.35-0.5 mm)

Fig 4. Effect of particle size on breakage probability of LC at different impact velocities

Fig 5. Effect of calcination temperature on different samples: (a) breakage probability; (b) reduction of Sauter mean diameter (original particle size range of 0.35-0.5 mm)

Fig 6. SEM images of LCF after first calcination at 850 ^{o}C for 15 min

Fig 7. Probability density function of particle size after impact: (a) LF calcined at 850 ^{o}C; (b) LCF calcined at 850 ^{o}C

Fig 8. Effect of multiple calcinations on different samples: (a) breakage probability; (b) reduction of Sauter mean diameter (carbonation at 650 ^{o}C for 20 min in 15% CO_2, calcination at 850 ^{o}C for 15 min in pure N_2)

Fig 9. SEM image of LCF after 11th calcination

Fig 10. Effect of multiple carbonations on different samples: (a) breakage probability; (b) reduction of Sauter mean diameter (carbonation at 650 ^{o}C for 20 min in 15% CO_2, calcination at 850 ^{o}C for 15 min in pure N_2)

Fig 11. Probability density function of particle size after impact: (a) LCF after 11th carbonation; (b) LCF after 11th calcination

Fig 12. d_0/d_{sv} as a function of v^2 for LCF before and after different reactions

Fig 13. BET surface area and pore volume distributions of LCF and LC during multiple cycles

Fig 14. SEM images of sorbents after calcination: (a), (b) LF after 1st calcination at 850 ^{o}C, (c) LCF after 1st calcination at 850 ^{o}C, (d) LCF after 1st calcination at 950 ^{o}C, (e) LCF after 11th calcination at 850 ^{o}C, (f) LC after 11th calcination at 850 ^{o}C (carbonation at 650 ^{o}C for 20 min in 15% CO_2 in the cycle test)

Figures

Figure 1

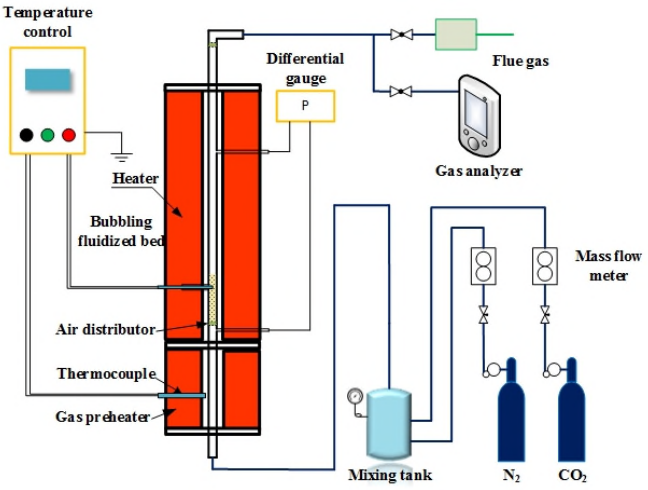

Figure 2

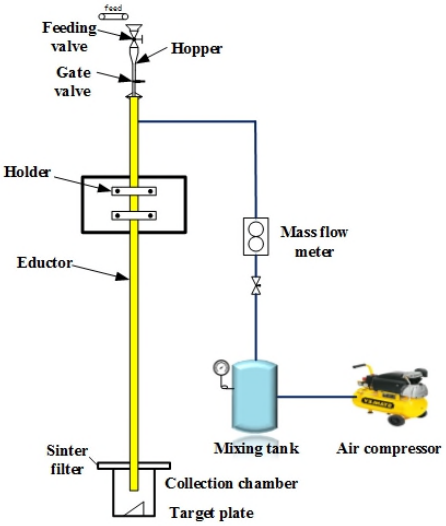

Figure 3

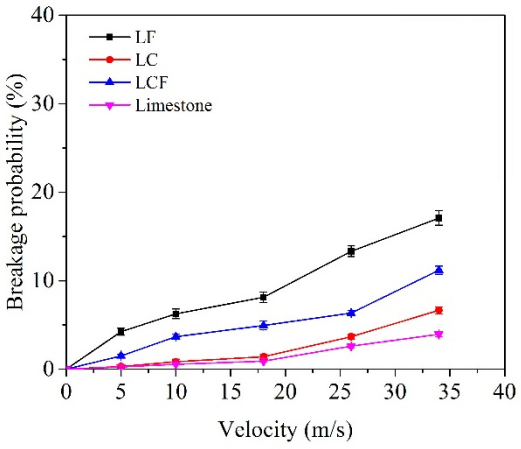

Figure 4

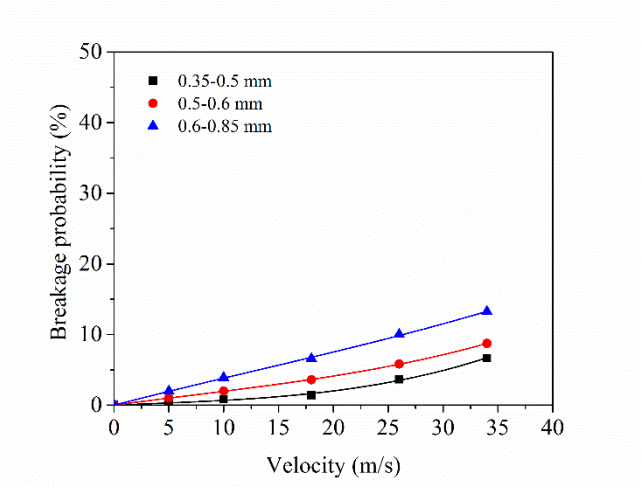

Figure 5

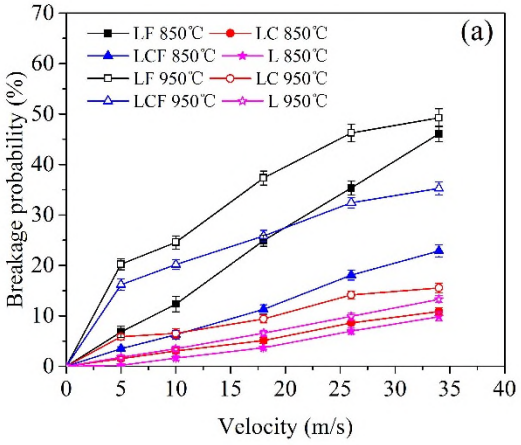

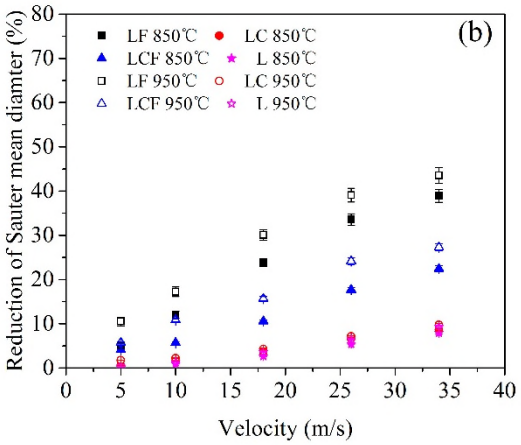

Figure 6

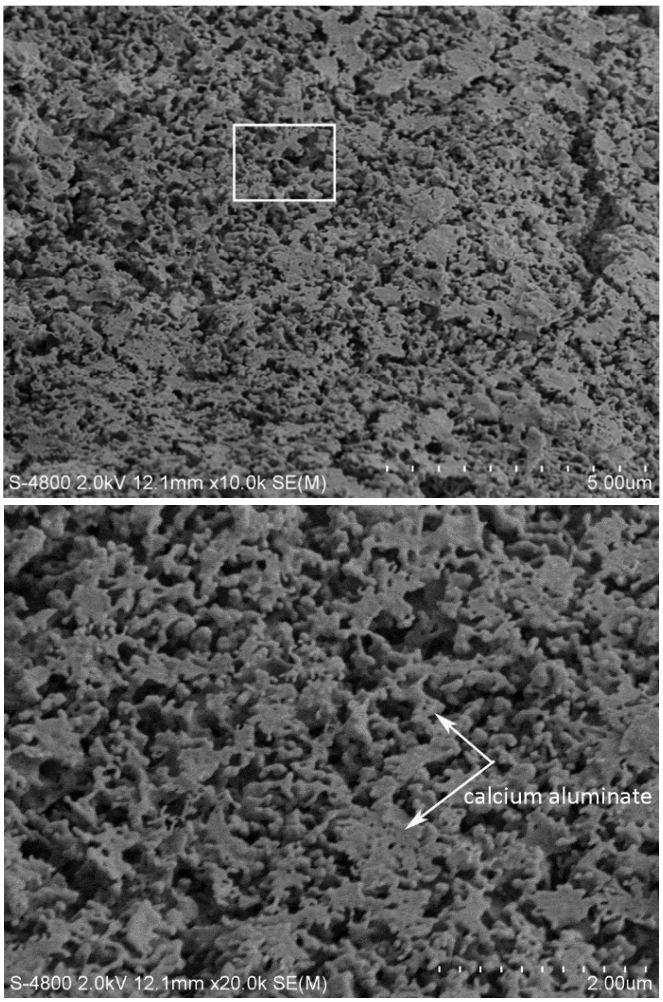

Figure 7

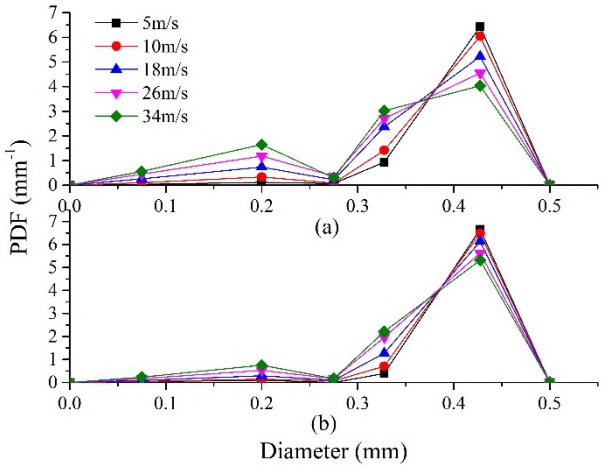

Figure 8

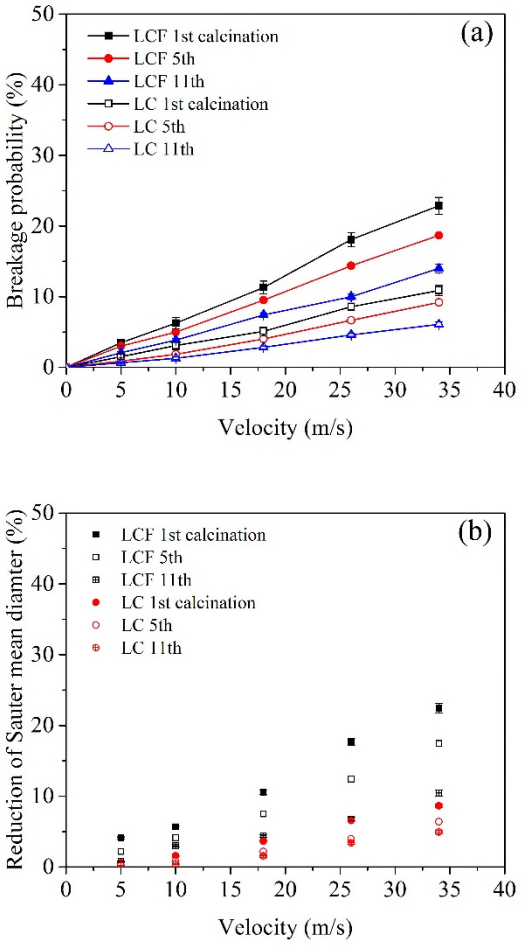

Figure 9

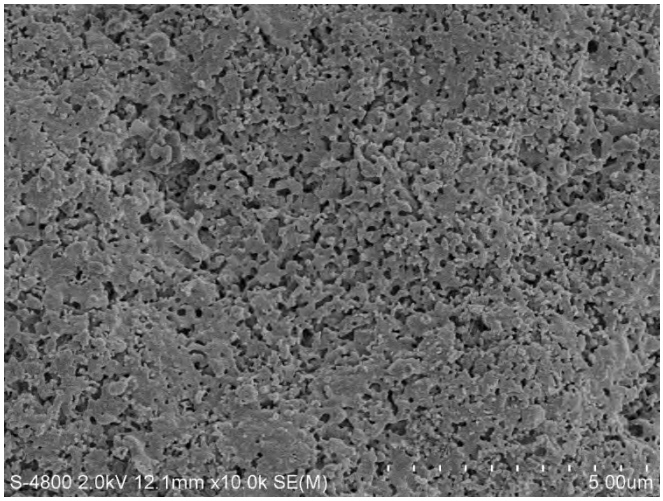

Figure 10

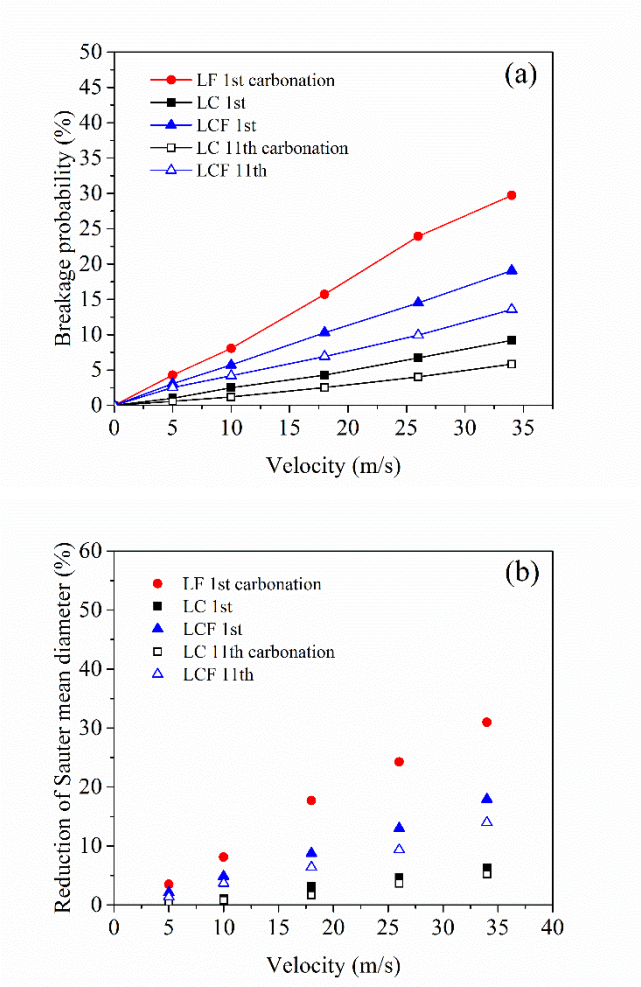

Figure 11

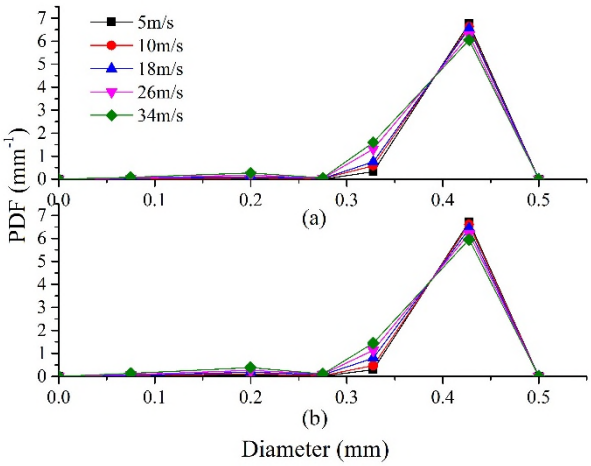

Figure 12

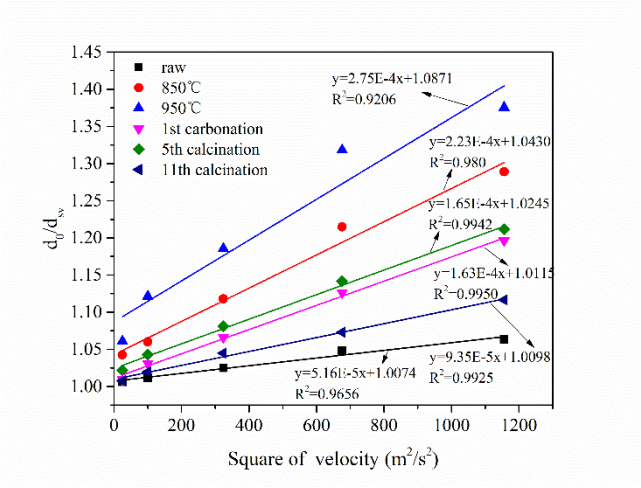

Figure 13

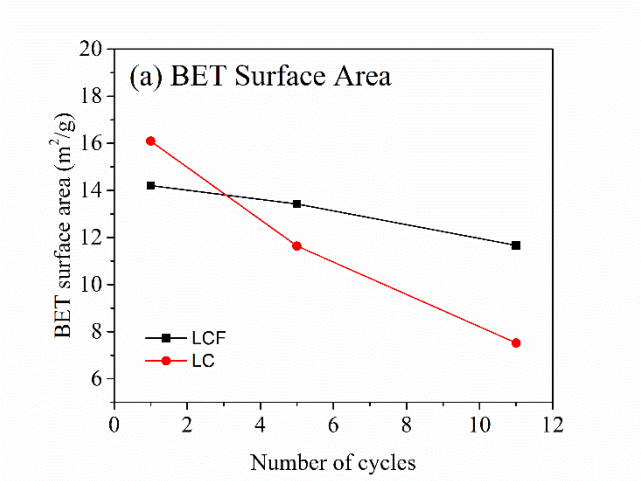

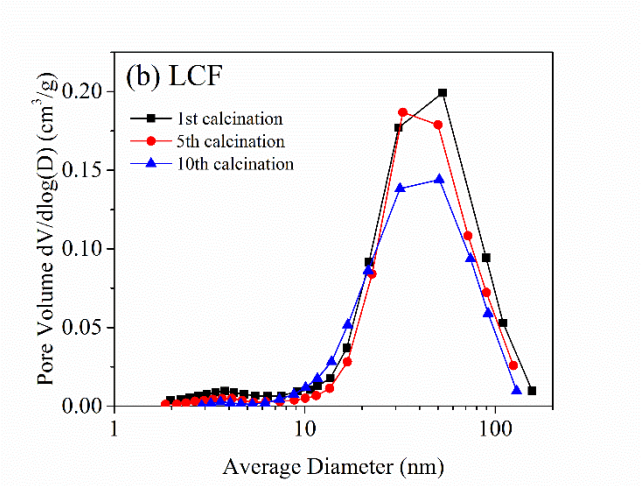

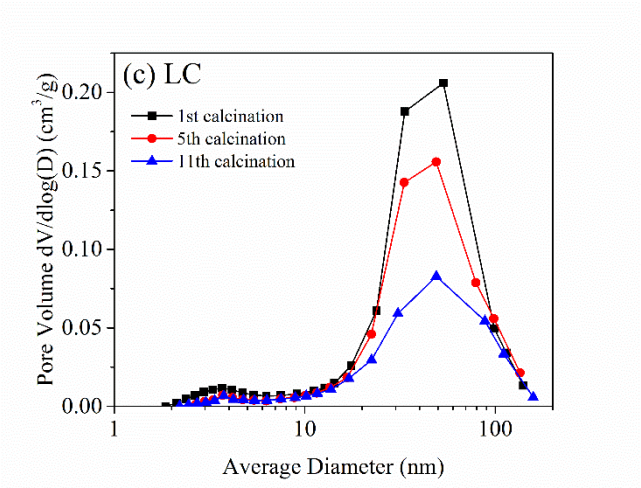
(c) LC
1st calcination
5th calcination
11th calcination
Pore Volume dV/dlog(D) (cm³/g)
0.00
0.05
0.10
0.15
0.20
1
10
100
Average Diameter (nm)

Figure 14

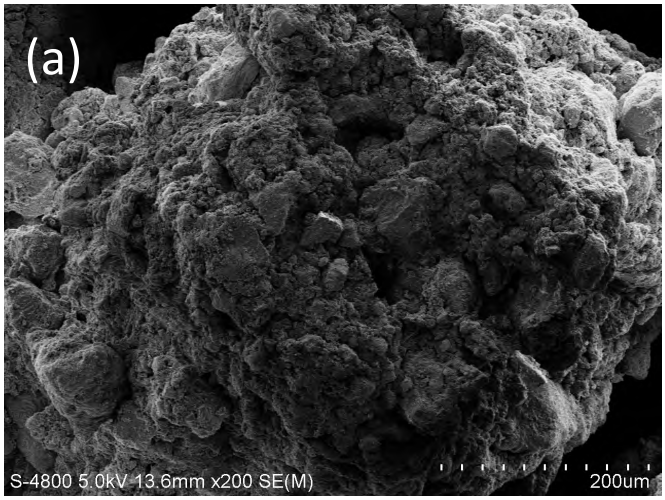
(a)
S-4800 5.0kV 13.6mm x200 SE(M)
200um

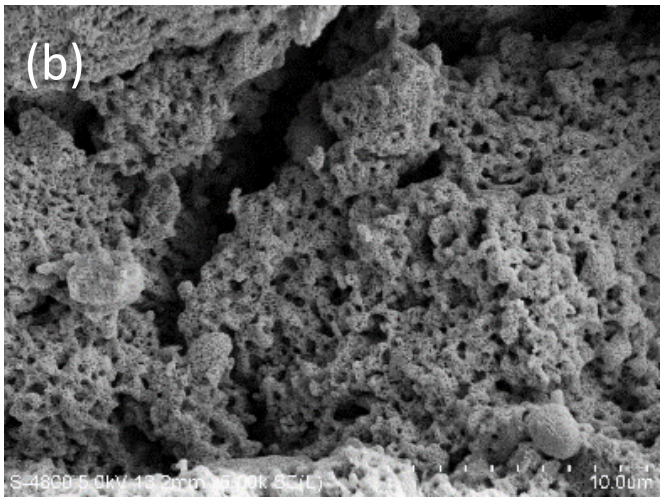
(b)
10.0um

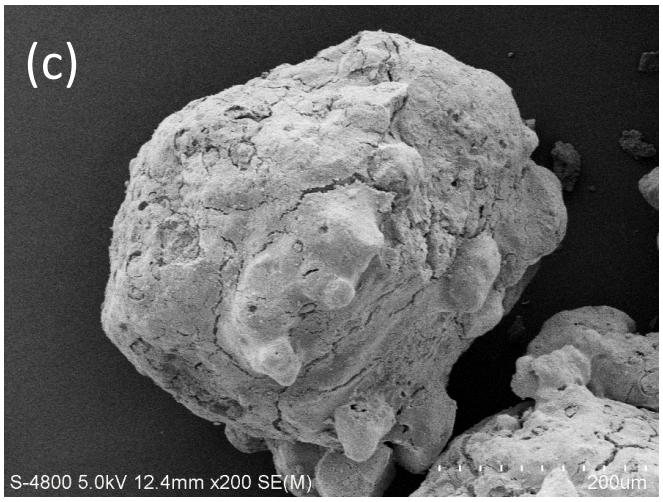
(c)
S-4800 5.0kV 12.4mm x200 SE(M)
200um

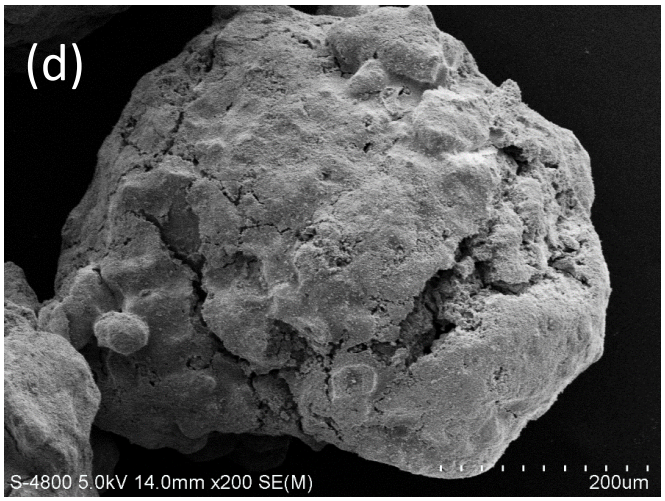
(d)
S-4800 5.0kV 14.0mm x200 SE(M)
200um

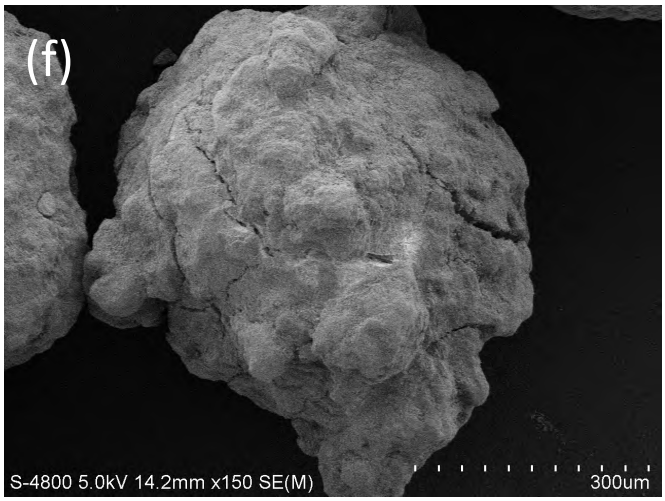

Table of Contents